Journal of Alloys and Compounds 501 (2010) 143–147

Contents lists available at ScienceDirect

Journal of Alloys and Compounds

journal homepage: www.elsevier.com/locate/jallcom

The effect of rare earth dopants on the structure, surface texture and photocatalytic properties of TiO_2–SiO_2 prepared by sol–gel method

R.M. Mohamed [a,b,*], I.A. Mkhalid [a]

[a] Chemistry Department, Faculty of Science, King Abdul Aziz University, Jeddah, Saudi Arabia
[b] Nanostructured Material Division, Advanced Materials Department, Central Metallurgical R&D Institute, Helwan, 11421 Cairo, Egypt

ARTICLE INFO

Article history:
Received 23 January 2010
Received in revised form 3 April 2010
Accepted 7 April 2010
Available online 20 April 2010

Keywords:
TiO_2–SiO_2
Rare earth
Photocatalytic
Oxidation
EDTA

ABSTRACT

The sol–gel method was successfully used to prepare a series of TiO_2–SiO_2 and rare earth (RE) (La^{3+}, Nd^{3+}, Sm^{3+}, Gd^{3+})-doped TiO_2–SiO_2 nanoparticles at a doping level of 3 atomic percent. The structural features of parent TiO_2–SiO_2 and RE–TiO_2–SiO_2 fired at 550 °C have been investigated by XRD, UV-diffuse reflection, SEM and nitrogen adsorption measurements at −196 °C. XRD data verified the formation of typical characteristic anatase form in all the prepared RE-doped TiO_2–SiO_2 samples. In comparison with the pure TiO_2–SiO_2 samples (ca. 35 nm in diameter), the RE–TiO_2–SiO_2 samples have relatively small particle size indicating that the doping with RE metal ions can improve the particle morphology, and retard the grain growth of TiO_2–SiO_2 during heat treatment. The results indicated that Gd^{3+} doped TiO_2–SiO_2 has the lowest bandgap and particle size compared with pure TiO_2–SiO_2 and other nanoparticles of RE-doped TiO_2–SiO_2. The highest surface area (S_{BET}) and pore volume (V_p) values were recorded for Gd–TiO_2–SiO_2 as well. The effect of doping on the photoactivity was evaluated by the photocatalytic degradation of EDTA as a probe reaction. Among all the pure and RE-doped TiO_2–SiO_2, Gd^{3+}–TiO_2–SiO_2 performed the highest catalytic activity towards the tested reaction. That might be due to its special characteristics of particle size, surface texture and bandgap properties. Details of the synthesis procedure and results of the characterization studies of the produced RE–TiO_2–SiO_2 are presented in this paper.

1. Introduction

During the recent decades, the photocatalytic application using semiconductors has received a lot of attention to solve the environmental problems [1–24]. TiO_2 has turned out to be the semiconductor with the highest photocatalytic activity, being non-toxic, stable in aqueous solution and relatively inexpensive [5]. The photocatalytic property of TiO_2 is due to its wide bandgap and long lifetime of photo generated holes and electrons. The high degree of recombination of the photo generated electrons and a hole is a major limiting factor controlling its photocatalytic efficiency and impeding the practical application of these techniques in the degradation of contaminants in water and air. Thus, a major challenge in heterogeneous photocatalysis is need to increase the charge separation efficiency of the photocatalysts [6].

In order to decrease the bandgap of parent titania photocatalyst (E_g = 3.2 eV), slow down the recombination rate of the e^-/h^+ pairs and enhance interfacial charge-transfer efficiency, the properties of TiO_2 have been modified by selective surface treatments such as surface chelation, surface derivatization, platinization, and by selective metal ions doping TiO_2 [9–13]. Coupled semiconductor photocatalysts exhibited a very high photocatalytic activity for both gas and liquid phase reactions. Researchers had much interest in coupling two semiconductor particles with different bandgap widths such as TiO_2-CdS, TiO_2-WO_3, TiO_2-SnO_2 [14,15], TiO_2–MoO_3 [16] TiO_2–SiO_2 aerogel [17] and TiO_2–Fe_2O_3 [18,21].

Lanthanide ions are known for their ability to form complexes with various Lewis bases (e.g. acids, amines, aldehydes, alcohols, thiols) in the interaction of these functional groups with the f-orbitals of the lanthanides. Although doping of lanthanide ions into TiO_2 attracted some attentions [22–26], such works are little so far. Incorporation of lanthanide ions into a TiO_2 matrix could provide a means to concentrate on the organic pollutant at the semiconductor surface and therefore enhance the photoactivity of titania [27–38].

The primary driving force in this work is to focus on the effect of RE dopants on the structure, bandgap, surface texture and their relation with the photocatalytic properties of TiO_2–SiO_2 prepared by sol–gel method. The photocatalytic properties have been investigated by employing the photo degradation of EDTA as a pattern of organic pollutant degradation reaction.

* Corresponding author at: Chemistry Department, Faculty of Science, King Abdul Aziz University, Jeddah, Saudi Arabia. Tel.: +966 540715648.
E-mail address: redama123@yahoo.com (R.M. Mohamed).

0925-8388/$ – see front matter © 2010 Elsevier B.V. All rights reserved.
doi:10.1016/j.jallcom.2010.04.061

2. Experimental

2.1. Materials

Tetraethylorthosilicate, Titanium isoporoxide, Neodymium nitrate hexahydrate, Samarium nitrate hexahydrate, Gadolinium (III) oxide and Lanthanum nitrate hexahydrate were used as precursors in the sol–gel preparations. Distilled water was used and all other chemicals were analytical grade.

The parent TiO_2–SiO_2 and RE-doped nanoparticles were prepared by sol–gel technique. The sol corresponds to the overall molar ratio of $Si(OC_2H_7)_4$:$Ti(C_4H_9O_4)$:C_2H_5OH:H_2O:HNO_3 = 4:1:20:4:0.001. In each case, Si $(OC_2H_7)_4$ and Ti $(C_4H_9O_4)$ were first dissolved in ethanol and water medium. The lanthanide salts were dissolved into stoichiometric amount of water and nitric acid and then added drop wise into the sol through stirring for 60 min at room temperature. The prepared sol was left to stand for the formation of gel. It was calcined at 550 °C for 5 hrs. The atomic ratio of Ti^{4+}:lanthanide ions were kept as 97:3 for all RE-doped nanoparticles.

2.2. Methods

X-ray powder diffraction (XRD) patterns were carried out at room temperature using a model Bruker axs, D8 Advance. Average crystallize size (D) of the obtained powders were calculated by X-ray line broadening technique performed on the direction of lattice using computer software based on the so-called Hall-equation–Scherer's formula $D = 0.89\lambda/\beta\cos\theta$ [39], where D is the crystallite size, λ represents the X-ray wavelength, θ is the Bragg's angle and β is the pure full width of the fraction line at half of the maximum capacity. The surface texture characteristics obtained from nitrogen adsorption isotherms were measured at −196 °C using a conventional volumetric apparatus. The specific surface area was measured using the BET method. The samples were thermally degassed at 300 °C prior to the adsorption measurements. The micropore volume and the external surface area were obtained from the t-plot. The bandgaps (E_g) of the samples were determined by using JASCO (V 570) software based on the so-called direct transition formula $\alpha h\gamma = \text{constant}(h\gamma - E_g)^n$ [40], where α is extinction coefficient [cm^{-1}]; γ is wave number [cm^{-1}]; h is the blank constant.

The photoactivity experiments were carried out in a cylindrical Pyrex glass reactor containing different loading of catalyst and 250 ml of aqueous solution of EDTA at 5×10^{-3}M concentration at 30 °C for 60 min. A 150 W medium pressure Hg lamp (254 nm) immersed within the photoreactor was used. The EDTA was determined by complexometeric titration with Zn^{2+} standard solution [40]. The removal efficiency of EDTA has been calculated by applying the following equation:

$$\%\,\text{removal efficiency} = (C^\circ - C)/C^\circ \times 100$$

where C° is the original EDTA content, C is the retained EDTA in the solution.

Before all photocatalytic runs, a fresh solution (250 ml) of EDTA were adjusted to the required pH, and the catalyst was suspended at 0.3 g/l concentrations. Suspensions were kept in dark and magnetically stirred at 30 °C for 60 min. The results indicate that adsorption efficiency was about 18–20%.

3. Results and discussion

3.1. Evaluation and characterization of synthesized material

3.1.1. XRD analysis

The crystalline phase of each parent TiO_2–SiO_2 and RE-doped TiO_2–SiO_2 nanoparticles prepared by sol–gel was determined by powder XRD and the phase changes are shown in Fig. 1. In parent TiO_2–SiO_2 and all RE-doped TiO_2–SiO_2 catalysts, the figure presents a group of lines at 2 theta values of 25.2, 37.5, 47.7, 53.3, 54.7 and 62° which are attributed to anatase phase [PDF # 71-1169]. However, no diffraction peaks of RE oxides in the patterns of RE-doped samples were observed. This is probably due to the low RE doping content (ca.3%) and the data may also imply that the RE oxides are well dispersed within the TiO_2–SiO_2 phase. The XRD data revealed that all the studied RE metal oxides inhibit the phase transformation from anatase to rutile during calcinations even at high temperatures (ca. 550 °C) while in other works, the anatase phase started to convert into rutile before 500 °C [41]. The crystallite size, calculated from Scherrer equation (D) of pure TiO_2–SiO_2 and RE-doped TiO_2–SiO_2 is listed in Table 1. The crystallite size value is ranging from 22 to 35 nm. Obviously, doping of TiO_2–SiO_2 with RE metal oxides leads to reducing the crystallite size of TiO_2–SiO_2 from 35 nm to 22 nm in Gd^{3+}–TiO_2–SiO_2. It is apparent that doping with rare earth metal oxides leads to lower agglomeration of crystals that produces smaller particle size. The least particle size was noticed for Gd–TiO_2–SiO_2 nanoparticles.

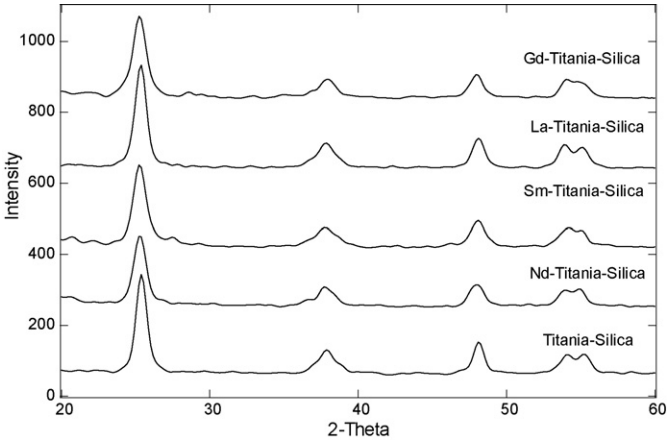

Fig. 1. XRD patterns of parent TiO_2–SiO_2 and RE–TiO_2–SiO_2 nanoparticles.

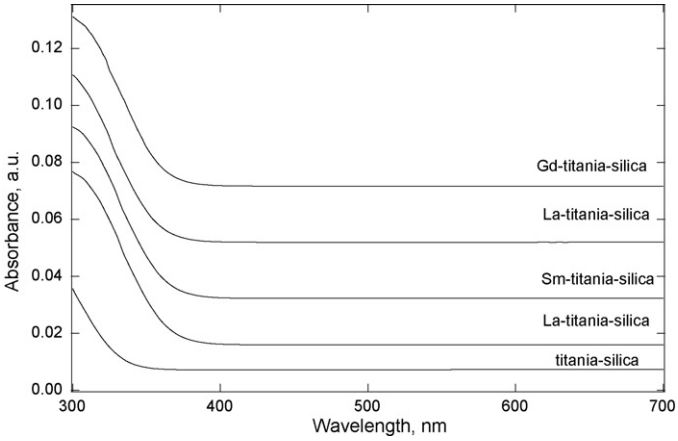

Fig. 2. Diffuse reflectance UV–vis absorption spectra of parent TiO_2–SiO_2 and RE–TiO_2–SiO_2 nanoparticles.

3.1.2. UV–vis spectroscopy

Fig. 2 depicts the diffuse reflectance UV–vis absorption spectra of TiO_2–SiO_2, Nd–TiO_2–SiO_2, Sm–TiO_2–SiO_2, La–TiO_2–SiO_2, and Gd–TiO_2–SiO_2. The main semiconductor properties are strongly dependant on the bandgap. The band gap plays a critical role in deciding the photocatalytic activity of photocatalysts because

Table 1
Effect of RE-doped TiO_2–SiO_2 on the photoactivity.

Sample	Crystallite size, nm	Band gap, eV	EDTA removal efficiency, %	V_p (cm^3/g)	Surface area, m^2/g
TiO_2–SiO_2	35	3.25	87.00	0.298	320
La–TiO_2–SiO_2	25	3.18	88.20	0.490	440
Nd–TiO_2–SiO_2	24	3.10	89.70	0.320	410
Sm–TiO_2–SiO_2	23	3.05	89.80	0.313	445
Gd–TiO_2–SiO_2	22	2.98	92.70	0.520	495

Table 2
Texture parameters of parent TiO_2–SiO_2 and RE–TiO_2–SiO_2 nanoparticles.

Sample	S_{BET} (m^2/g)	S_t (m^2/g)	S_{micro} (cm^2/g)	S_{meso} (cm^2/g)	S_{ext} (cm^2/g)	V_p (cm^3/g)	V_{micro} (cm^3/g)	V_{meso} (cm^3/g)	r^- (Å)
TiO_2–SiO_2	320	360	33	300	33	0.298	0.288	0.010	31.72
La–TiO_2–SiO_2	440	462	77	380	44	0.490	0.410	0.080	38.16
Nd–TiO_2–SiO_2	410	348	37	380	22	0.320	0.290	0.030	27.88
Sm–TiO_2–SiO_2	445	462	93	370	34	0.313	0.257	0.066	40.30
Gd–TiO_2–SiO_2	495	510	97	400	40	0.520	0.450	0.070	37.40

Note: S_{BET}, BET-surface area; S_t, surface area derived from V_{l-t} plots; S_{micro}, surface area of micropores; S_{meso}, surface area of micropores; S_{ext}, external surface area; V_p, total pore volume; V_{micro}, pore volume of micropores; V_{meso}, pore volume of mesopores; r^-, mean pore radius.

it participates in determining the e^-/h^+ recombination rate. It was estimated by the diffuse reflectance absorption spectrum and summarized in Table 1. The bandgap was 3.25, 3.18, 3.10, and 3.05 to 2.98 eV for the samples TiO_2–SiO_2, Nd–TiO_2–SiO_2, Sm–TiO_2–SiO_2, La–TiO_2–SiO_2, and Gd–TiO_2–SiO_2, respectively. It is clear that doping with RE ions has a great advantage, namely the decrease in the bandgap of TiO_2–SiO_2, which has a pronounced effect of the semi-conduction properties of the prepared nanoparticles.

3.1.3. Specific surface area trends

The surface parameters of surface area and the data calculated from the *t*-plot were estimated by the low-temperature nitrogen adsorption at relative pressures (P/P^0) in the range of 0.05–0.9 and are given in Table 2. The N_2 adsorption isotherms (not shown) for the parent and the RE-doped TiO_2–SiO_2 are typical of mesoporous solids, however, an increase in the adsorption capacity of the TiO_2–SiO_2 was observed after introducing RE ions. The surface area changed from 320 to 495 m^2/g in case of Gd^{3+}–TiO_2–SiO_2 (≈ 55% increase of surface area compared to the parent TiO_2–SiO_2). It is worth mentioning that the S_{BET} values of the prepared catalysts are relatively higher than those of other analogues samples as mentioned in literature [43]. Furthermore, the total pore volume of RE–TiO_2–SiO_2 is twice that of TiO_2–SiO_2. Since the TiO_2 (anatase) structure is not affected by doping with RE ions as revealed by XRD, the large increase of surface area and mesopore volume observed

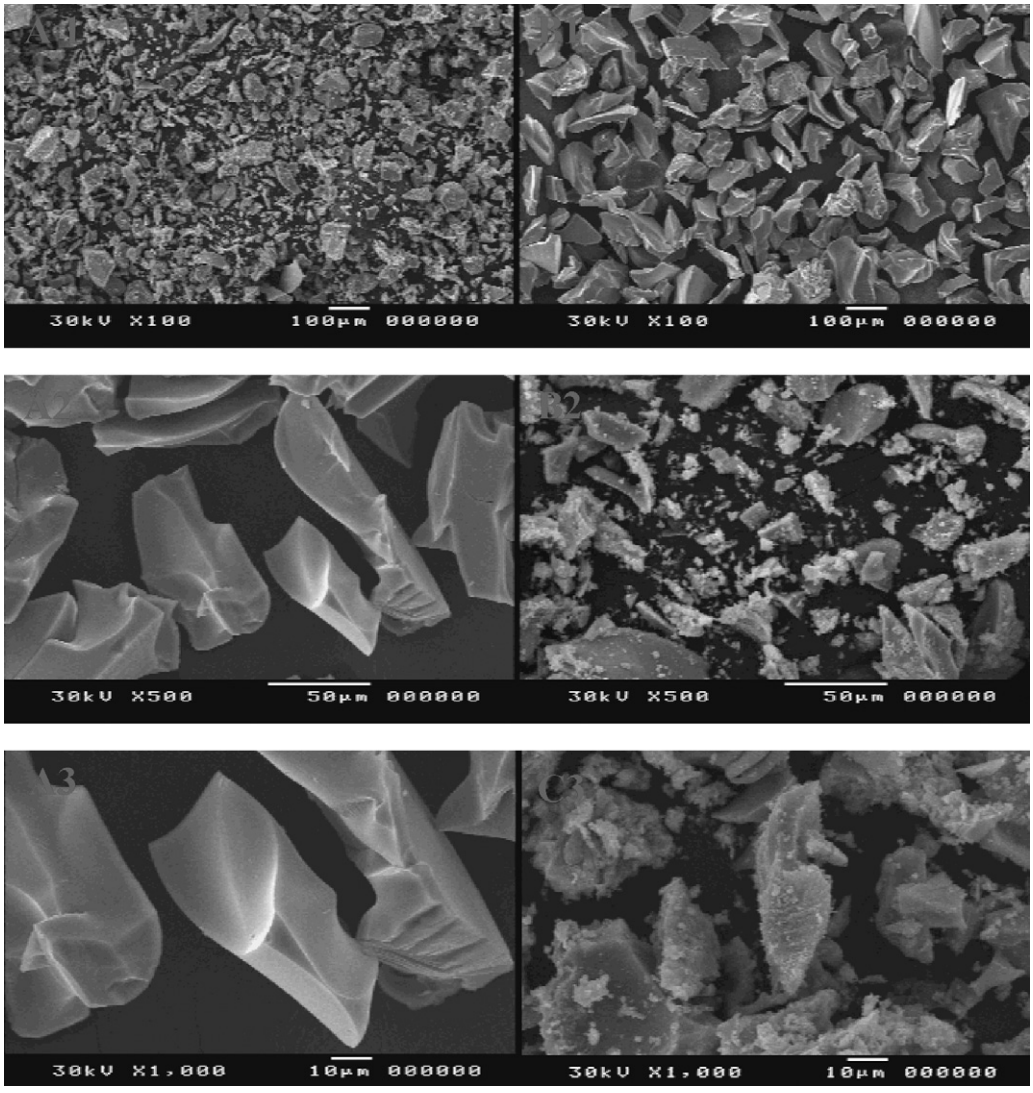

Fig. 3. SEM surface morphology of TiO_2–SiO_2 (A), and Gd–TiO_2–SiO_2 (B), at different magnifications, where magnifications are 100×, 500× and 1000× for (A1, B1), (A2, B2) and (A3, B3) respectively.

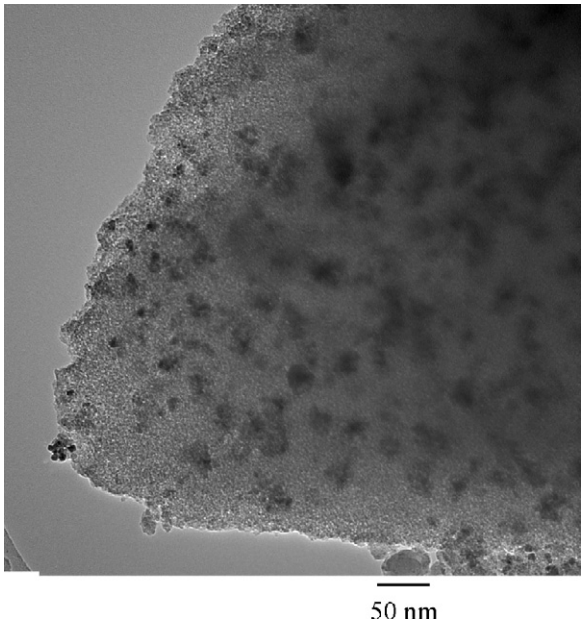

Fig. 4. TEM image of Gd–TiO_2–SiO_2.

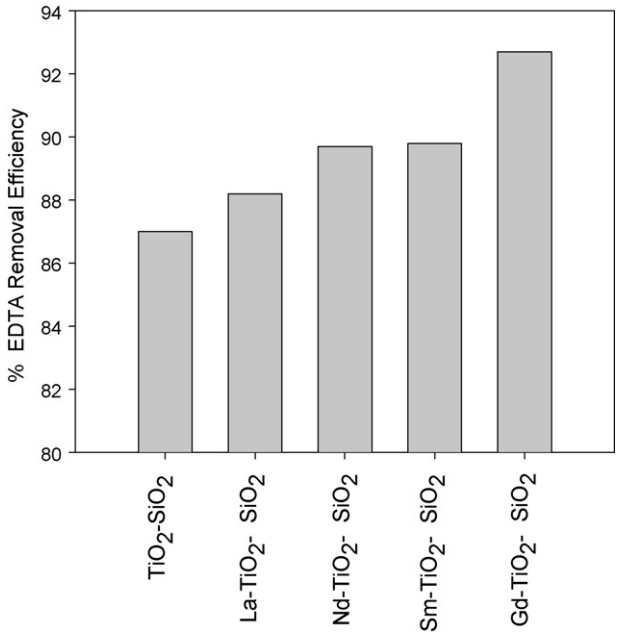

Fig. 5. Effect of type of RE-doped TiO_2–SiO_2 on EDTA removal efficiency %.

for the RE-doped TiO_2–SiO_2 is interpreted as arising from the formation of mesoporous texture as a result of the sol–gel preparation method. Further data assessment reveals that, the values of S_{BET} and S_t are generally close in most samples indicating the presence of mesopores. The values of external surface area (S_{ext}) of the samples are very small which is indicative of the porous nature of these solids. The values of S_{meso} are high compared to that of S_{micro} implying that the main surface is mesoporous solid as represented by the isotherm. The surface texture data will be correlated with the catalytic activity as will be mentioned later on.

3.1.4. SEM observation

Surface morphology of TiO_2–SiO_2 and Gd–TiO_2–SiO_2 was studied as well using SEM micrograph. Fig. 3 shows that the shape of the particles does not show much difference. This means that the 3% addition of RE is not effective for changing the morphology of TiO_2–SiO_2.

3.1.5. TEM observation

Fig. 4 shows TEM of Gd–TiO_2–SiO_2. The results show that Gd was well dispersed within the TiO_2–SiO_2 phase, which is agreement with XRD results.

3.2. Photocatalytic activity studies

The photocatalytic degradation of EDTA was used as a probe reaction to test the catalytic activity of the prepared nanoparticles. Fig. 5 shows the effect of RE-doped TiO_2–SiO_2 nanoparticles on photocatalytic oxidation of EDTA after 60 min. at room temperature using 5×10^{-3} M of EDTA at pH 3 and 0.3 g catalyst/1000 ml EDTA solution. The data showed that the photocatalytic activities of the RE-doped TiO_2–SiO_2 nanoparticles were higher than those of parent TiO_2–SiO_2. Knowing that, the pure RE oxides did not have photocatalytic oxidation properties, such variation in activity must be due to the differences in interaction between RE oxides and TiO_2–SiO_2 that led to several modifications in physical properties such as bandgap, particle size and surface texture. The catalytic activity of TiO_2–SiO_2 generally increased with the addition of rare earth promoters. It reached the maximum in case of Gd–TiO_2–SiO_2.

Table 1 demonstrates the correlation between the photoactivity and the physical properties such as bandgap, surface area and pore volume. It is clear that, the photocatalytic activity reached the maximum in case of Gd–TiO_2–SiO_2 in which the surface area and pore volume reached the maximum but the bandgap was at a minimum. Table 1 shows the good correlation between the bandgap, surface area and pore volume with the catalytic activity where the activity was gradually increased with the decrease of bandgap and the increase of both the surface area and pore volume.

The results showed that the photocatalytic activities of the rare earth doped titania–silica nanoparticles increased with decreasing the bandgap. This is due to decrease energy to exit electron from conduction band to valance band. Also, the Gd^{3+}–TiO_2–SiO_2 has the best photoactivity, since it has the lowest bandgap and particle size and the highest surface area and pore volume.

3.2.1. Effect of pH

A series of experiments have been carried out to study the effect of pH on EDTA removal efficiency under the following conditions: 0.3 g/l catalyst/EDTA solution ratio; 5×10^{-3} M Conc. of EDTA; and 1 h reaction time. The findings are summarized in Table 3. The results indicate that increasing pH of EDTA solution from 3 to 7 leads to increasing EDTA removal efficiency from 92.1% to 97.5%, but at pH more than 7, the EDTA removal efficiency almost remains unchanged in both two methods. The possible reason for this behavior is that alkaline pH range favours the formation of more OH radical due to the presence of large quantity of OH^- ions in the alkaline medium, which enhances the photocatalytic degradation of EDTA significantly [42]. The optimum condition for pH in 7 at 97.5% photodegradation of EDTA.

Table 3
Effect of pH of EDTA solution on EDTA removal efficiency.

pH of EDTA	EDTA removal efficiency, %
3	92.7
4	95.7
7	97.5
9	97.9

Table 4
Effect of EDTA concentration on EDTA removal efficiency.

EDTA concentration, M	EDTA removal efficiency, %
5×10^{-5}	97.5
5×10^{-4}	97.5
5×10^{-3}	97.5
7.5×10^{-3}	82.4
5×10^{-2}	52.6

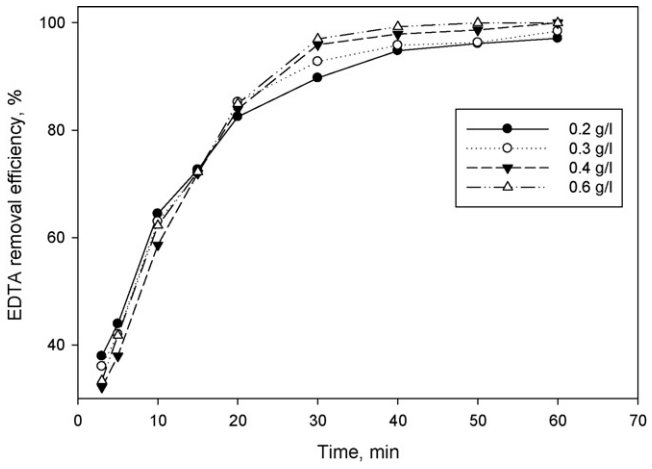

Fig. 6. Effect of photocatalyst weight on EDTA removal efficiency %.

3.2.2. Effect of EDTA concentration

A series of experiments have been carried out to study the effect of the EDTA concentration on EDTA removal efficiency under the aforementioned conditions at pH 7. The results summarized in Table 4. It can be seen that increasing EDTA concentration from 5×10^{-5} to 5×10^{-3} M, has no significant effect on EDTA removal efficiency, but at a concentration higher than 5×10^{-3} M, the EDTA removal efficiency was decreased. The optimum conditions for EDTA concentration are 5×10^{-3} M at EDTA removal efficiency 97.5%.

3.2.3. Effect of catalyst/EDTA, solution ratio

A series of experiments have been carried out to study the effect of catalyst/EDTA solution ratio g/l on EDTA removal efficiency under the aforementioned conditions at EDTA concentration is 5×10^{-3} M. The findings are shown in Fig. 6. The results indicate that increasing catalyst/EDTA solution ratio from 0.2 to 0.4 g/l, leads to increasing EDTA, the removal efficiency from 97.5% to 99.9% respectively, but at catalyst/EDTA solution ratio more than 0.4 g/l the EDTA removal efficiency almost remains unchanged. The optimum condition of catalyst/EDTA solution ratio, g/l is 0.4 at 99.9% EDTA removal efficiency.

4. Conclusions

The sol–gel method is useful for the preparation of nanostructured RE–TiO_2–SiO_2 with high photocatalytic activity, high surface area and desirable pore structures. A series of Nd, Sm, Gd, and La homogenously doped nanocrystalline TiO_2–SiO_2 have been successfully synthesized by sol gel method. The type of dopant rare earth showed significant effect on the texture structure, bandgap and particle size. These physical changes affected the efficiency of the photo degradation of EDTA. The activity is well correlated with the bandgap, surface area and pore volume. In addition, the differences in catalytic activity are due to the change in the amount of surface hydroxyl groups resulting from the interaction between the rare earth oxides and TiO_2–SiO_2. The Gd–TiO_2–SiO_2 nanoparticles presented the highest photoactivity due to its high surface area, large pore volume, small particle size and small bandgap.

References

[1] P.C. Calza, C. Minero, E.S. Rodrigues, K.T. Ranjit, S. Uma, I.N. Martyanov, K.J. Klabunde, Adv. Mater. 17 (2005) 2467.
[2] H. Kisch, W. Macyk, ChemPhysChem 3 (2002) 399.
[3] A.P. Davis, D.L. Green, Environ. Sci. Technol. 33 (1999) 609.
[4] H. Choi, A.C. Sofranko, D.D. Dionysiou, Adv. Funct. Mater. 16 (2006) 1067.
[5] A. Braun, in: E. Pelizzetti, M. Schiavello (ed.), Photo chemical Conversion and storage of solar energy, Kluwer, Dordrecht, 1991, p. 551.
[6] H. Hidaka, Y. Asai, J. Zhao, K. Nohara, E. Pelizzetti, N. Serpone, J. Phys. Chem. 99 (1995) 8244.
[7] L. Kruczynski, H.D. Gesser, C.W. Turner, E.A. Speer, Nature 291 (1981) 399.
[8] J. Moser, S. Punchihewa, P.P. Infelta, M. Gratzel, Langmuir 7 (1991) 3012.
[9] A.P. Hong, D.W. Bahnemann, M.R. Hoffmann, J. Phys. Chem. 91 (1987) 2109.
[10] J. Lin, J. Yu, S.K. Lam, J. Catal. 183 (1999) 368.
[11] Y. Zhao, C. Li, X. Liu, F. Gu, J. Alloys Compd. 440 (2007) 281.
[12] H. Xia, H. Zhuang, D. Xiao, T. Zhang, J. Alloys Compd. 465 (2008) 328.
[13] Y. Yan, X. Qiu, H. Wang, L. Li, X. Fu, L. Wu, G. Li, J. Alloys Compd. 460 (2008) 491.
[14] I. Shiyanovskaya, M. Hepel, J. Electrochem. Soc. 145 (1998) 3981.
[15] N. Serpone, P. Maruthamuthu, P. Pichat, E. Pelizzetti, H. Hidaka, J. Photochem. Photobiol. A: Chem. 85 (1995) 247.
[16] K.Y. Song, M.K. Park, Y.T. Kwon, H.W. Lee, W.J. Chung, W.I. Lee, Chem. Mater. 13 (2001) 2349.
[17] A.A. Ismail, I.A. Ibrahim, M.S. Ahmed, R.M. Mohamed, H. El-Shall, J. Photochem. Photobiol. A: Chem. 163 (2004) 445.
[18] B. Pal, T. Hata, K. Goto, G. Nogami, J. Mol. Catal. A: Chem. 169 (2001) 147.
[19] A.A. Ismail, Appl. Catal. B 58 (2005) 115.
[20] K.N.P. Kumar, A. Burggraaf, J. Mater. Chem. 3 (1993) 141.
[21] R. Gopalan, Y.S. lin, Ind. Eng. Chem. Res. 34 (1995) 1189.
[22] G. Boschloo, A. hagfeldt, Chem. Phys. Lett. 370 (2003) 381.
[23] A. Xu, Y. Gao, H. Liu, J. Catal. 207 (2002) 151.
[24] D.J. Bjorkert, R. Mayappan, D. Holland, M.H. Lewis, J. Euro. Ceram. Soc. 19 (1999) 1847.
[25] M.S.P. Francisco, V.R. Mastelaro, Chem. Mater. 14 (2002) 2514.
[26] C.P. Sibu, K.S. Rajesh, P. Mukundan, K.G.K. Warrier, Chem. Mater. 14 (2002) 2876.
[27] K.T. Ranjit, I. Willner, S.H. Bossmann, A.M. Braun, Environ. Sci. Technol. 35 (2001) 1544.
[28] J. lin, J.C. Yu, J. Photochem. Photobiol. A: Chem. 116 (1998) 63.
[29] D.W. Hwang, J.S. Lee, W. li, S.H. Oh, J. Phys. Chem. B 107 (2003) 4963.
[30] Y.H. Zhang, H.X. Zhang, Y.X. Xu, Y.G. Wang, J. Mater. Chem. 13 (2003) 2261.
[31] C.A. LeDuc, J.M. Campbell, J.A. Rossin, Ind. Eng. Chem. Res. 35 (1996) 247.
[32] B. Liang, S. Mianxin, Z. Tianliang, Z. Xiaoyong, D. Qingqing, J. Rare Earths 27 (2000) 461.
[33] Saepurahman, M.A. Abdullah, F.K. Chong, J. Hazard. Mater. 176 (2010) 451.
[34] V. Stengl, S. Bakardjieva, N. Murafa, Mater. Chem. Phys. 114 (2009) 217.
[35] J. Li, X. Yang, X. Yu, L. Xu, W. Kang, W. Yan, H. Gao, Z. Liu, Y. Guo, Appl. Surf. Sci. 255 (2009) 3731.
[36] J. Xu, Y. Ao, D. Fu, C. Yuan, J. Hazard. Mater. 164 (2009) 762.
[37] U.G. Akpan, B.H. Hameed, Appl. Catal. A 375 (2010) 1.
[38] T. Nguyen-Phan, M. Bock Song, E. Jung Kim, E. Woo Shin, Micropor. Mesopor. Mater. 119 (2009) 290.
[39] P. Tyagi, A.G. Vedeshwar, Bull. Mater. Sci. 34 (2001) 297.
[40] C.W. Schlapfer, N.N. Vlasova, S.K. Poznyak, A.I. Kokoring, J. Colloid Interface Sci. 239 (2001) 200.
[41] R.D. Shannon, Acta Crystallogr. A 32 (1976) 751.
[42] S. Monticone, R. Tufeu, V.A. Kanaev, E. Scolan, C. Sanchez, Appl. Surf. Sci. 162–163 (2000) 565.
[43] P. Yang, C. Lu, N. Hua, Y. Du, Mater. Lett. 57 (2002) 794.